encit 2020

ABCM Associação Brasileira de Engenharia e Ciências Mecânicas

18th Brazilian Congress of Thermal Sciences and Engineering
November 16–20, 2020 (Online)

ENC-2020-0208
PARAMETRIC DETERMINATION OF FUEL CONSUMPTION DURING CRUISE FLIGHT FOR FUEL CELL POWERED AIRPLANES

Guilherme N. Barufaldi
Roberto Gil A. da Silva
Instituto Tecnológico de Aeronáutica, Praça Mal. Eduardo Gomes, 50, Vila das Acácias, CEP: 12228-900, São José dos Campos – SP – Brazil
guilherme.barufaldi@protonmail.com, gil@ita.br

Abstract. *In the last decades, electric airplanes have become a topic of great interest for the aeronautical community. With increasing pressures to lower pollutant emissions, the aerospace industry has turned its attentions to the development of the so called green aircraft – vehicles that are more fuel-efficient. Electric airplanes are seen as one of the most promising solutions to this problem. However, since the propulsion system is distinct from internal combustion engines, performance characteristics can differ significantly from that of regular aircraft. One of the main factors that contribute to this difference is the power source that feeds electric energy to the motor. Fuel cells are one of the main embedded power sources employed to provide electricity in vehicles, and its use in airplanes is currently being researched. This work presents an analytical investigation of the fuel and oxidizer consumption during the cruise flight all-electric aircraft powered by fuel cells. This investigation is relevant because cruise flight usually is the crucial phase that drives aircraft design requirements. Parametric models are provided for the airplane aerodynamics, the propeller, the fuel cell and the electric motor. Analytical solutions are derived in parametric form, allowing quick calculations and eliminating the need for numerical solvers and possible convergence issues. Also, numerical results are provided to illustrate the method developed in the article.*

Keywords: *Electric aircraft, fuel cell, flight performance, green aircraft, aircraft conceptual design*

1. INTRODUCTION

In the last decades, electric airplanes have become a topic of great interest for the aeronautical community. With increasing pressures to lower pollutant emissions, the aerospace industry has turned its attentions to the development of the so called green aircraft – vehicles that are more fuel-efficient. Electric propulsion is currently seen as one of the main solutions to this problem and, with the continuous improvements in battery and fuel cell technologies, and electric motors and control systems, manned airplanes equipped with this type of propulsion are beginning to emerge in the general aviation market segment, e.g. (Schemp-Hirth, 2012), and (Boeing, 2015).

Although electric motors are not new, the study of electric aircraft performance is still being established. Since the propulsion system is different from internal combustion engines, performance characteristics and operational issues can differ significantly from that of regular aircraft (Sachs, 2012). One of the main factors that contribute to this is the power source that feeds electric energy into the motor. Fuel cells are one of the main embedded power sources employed to provide electricity in vehicles, and its use in airplanes is currently being researched, with a few successful airplanes having already flown.

A fuel cell is an electrochemical device that converts energy from a fuel and an oxidizing agent into electricity through redox reactions. The main difference between these devices and batteries is the fact that fuel cells work with a flow of substances being injected into the apparatus, contrary to batteries, where the substances and electrodes are statically stored into the structure (except in the case of flow batteries). Fuel cells have been used in aerospace applications since the mid-1960s, to generate power for satellites and space capsules, notably the command and service modules of the Apollo Spacecraft (Kelly, 2001).

In 2008, the Boeing HK-36 FCD flew for the first time (Lapeña-Rey *et al.*, 2010). This experimental motor glider was the first manned fuel-cell-powered airplane ever to fly, being equipped with both Li-ion batteries and hydrogen fuel cells. Since then, a few other aircraft powered by fuel cells have been flown, such as the DLR HY4 (DLR, 2016), but the output power limitations still severely constrain the usage of these power sources in commercial applications. Still, recent developments of fuel cell technology have shown that these devices not only constitute a viable option for commercial vehicles, but may offer serious competition even to advanced batteries (Caldwell, 2020).

This work presents an analytical investigation of the fuel and oxidizer consumption during the cruise flight of all-

electric aircraft powered by fuel cells. This investigation is relevant not only because every airplane must meet certain cruise performance requirements, such as fuel consumption, but also because it usually is the crucial phase for the aircraft design process. For most general aviation aircraft – the focus of the present study – the cruise phase happens with steady conditions, hence the analysis is conducted according to this assumption. Analytical expressions for fuel consumption are derived and presented in parametric form. The main objective is to provide tools and a theoretical framework for performance analysis, and for the conceptual design of such airplanes.

2. SYSTEM MODELS

2.1 Longitudinal Dynamics

In this work, a regular cruise flight with leveled wings is assumed, i.e., no lateral or directional movements occur. Hence, the longitudinal dynamic model of the aircraft is sufficient, and it is resumed by the following equilibrium equations (Nelson, 1998):

$$T = D + W \sin\gamma \tag{1}$$

$$L = W \tag{2}$$

where W is the aircraft weight; γ is the flightpath angle; T is the propeller thrust. The lift force L and the drag force D are given by Eqs. (3) and (4), respectively:

$$L = \frac{\rho V^2}{2} S C_L \tag{3}$$

$$D = \frac{\rho V^2}{2} S C_D \tag{4}$$

where V is the aircraft velocity (true airspeed); ρ is the air density; S is the wing reference area; C_L is the dimensionless lift coefficient; and C_D is the dimensionless drag coefficient. It is worth mentioning that, according to the Standard Atmosphere model (NASA/NOAA/USAF, 1976), there is a biunivocal correspondence between the altitude h and the air density ρ, hence for a given value of ρ, there is only one corresponding altitude h. Since electric airplanes fly at moderate to low airspeeds, compressibility effects can be neglected and C_D is modeled as a function of the lift coefficient only (Anderson, 1999).

$$C_D = f(C_L) \tag{5}$$

where f is a continuous function known as "drag polar." From Eqs. (2) and (3), one can conclude that, for given values of altitude and velocity, there is only one possible value of C_L.

2.2 Propeller Model

The aircraft is assumed to be equipped with a fixed-pitch propeller, which is usual in small airplanes and UAVs, due to its simplicity and lighter weight (Keane *et al.*, 2017). The propeller thrust T and its aerodynamic torque Q_{pr} are given by the following equations:

$$T = \rho C_T \left(\frac{\Omega}{2\pi}\right)^2 d^4 \tag{6}$$

$$Q_{\text{pr}} = \rho C_Q \left(\frac{\Omega}{2\pi}\right)^2 d^5 \tag{7}$$

where C_T and C_Q are the propeller thrust and torque coefficients, respectively; Ω is the rotational speed; and d is the propeller diameter. According to Mises (1945), both C_T and C_Q can be modeled by quadratic functions. Since the propeller is assumed to be known, C_T and C_Q can be expressed as functions of V and Ω:

$$C_T = -\frac{4\pi^2 a_T}{d^2}\left(\frac{V}{\Omega}\right)^2 + \frac{2\pi b_T}{d}\left(\frac{V}{\Omega}\right) + c_T \tag{8}$$

$$C_Q = -\frac{4\pi^2 a_Q}{d^2}\left(\frac{V}{\Omega}\right)^2 + \frac{2\pi b_Q}{d}\left(\frac{V}{\Omega}\right) + c_Q \tag{9}$$

where a_T, a_Q, b_T, b_Q, c_T, c_Q, are real constants that define the characteristic curves of a given fixed-pitch propeller. With the exception of b_T and b_Q, which may be negative, the constants are positive.

2.3 Fuel Cell Model

The fuel consumption calculation requires the knowledge of the chemical equations, hence the type of fuel cell must be known *a priori*. In this article, in order to illustrate the calculation procedure, a hydrogen-oxygen (H_2/O_2) proton exchange membrane (PEM) fuel cell is used as an example, as it is the most common type in use for aircraft. However, the rationale can be employed for other fuel cell types as well. The chemical reactions that take place at the anode and cathode are given by (O'Hayre *et al.*, 2009):

$$\text{anode:} \quad 2H_2 \rightarrow 4H^+ + 4e^- \tag{10}$$

$$\text{cathode:} \quad O_2 + 4e^- \rightarrow 2O^{2-} \tag{11}$$

From Eqs. (10) and (11), the stoichiometric proportions between reactants and electrons e^- are given by:

$$n_{H_2} = n_{e^-}/2 \tag{12}$$

$$n_{O_2} = n_{e^-}/4 \tag{13}$$

In Eqs. (12) and (13), the stoichiometric coefficients can be substituted by the relations between mass and molar mass ($n = m/M$) or between electric charge and the Faraday constant, yielding:

$$m_{H_2} = \frac{M_{H_2} C_{el}}{2F} \tag{14}$$

$$m_{O_2} = \frac{M_{O_2} C_{el}}{4F} \tag{15}$$

where m_{H_2} and m_{O_2} are the consumed masses of hydrogen and oxygen; M_{H_2} and M_{O_2} are the hydrogen and oxygen molar masses, respectively; C_{el} is the electric charge consumed; and F is the Faraday constant. Differentiating the functions in Eqs. (14) and (15) with respect to time yields:

$$\dot{m}_{H_2} = \frac{M_{H_2}}{2F} \cdot i \tag{16}$$

$$\dot{m}_{O_2} = \frac{M_{O_2}}{4F} \cdot i \tag{17}$$

The mass flows calculated with Eqs. (16) and (17) are based on the stoichiometric proportions of the chemical reactions, i.e., with a reaction yield of 100%. However, these reactions may not happen in this exact proportion due to mass transport phenomena and, therefore, reaction yield factors η_{ano} and η_{cat} are introduced, for the anode and the cathode, respectively. Hence, the total fuel and oxidizer mass flow $\dot{m}$, as a function of the output electric current, is calculated according to Eq. (18):

$$\dot{m} = \left(\frac{M_{H_2}}{2F\eta_{ano}} + \frac{M_{O_2}}{4F\eta_{cat}} \right) \cdot i \tag{18}$$

2.4 Electric Motor Model

The DC electric motor is modeled by an equivalent circuit diagram, depicted in Fig. 1, where U is the DC voltage applied to motor electric terminals; R_m is the motor internal resistance; i is the electric current flowing through the circuit; U_m is the motor counter-electromotive force; Q_m is the motor torque, in reaction to the load applied to the shaft by the propeller; and Ω is the motor rotational speed. In the present work no gearbox is considered, so both motor and propeller have equal rotational speeds.

The motor model is represented in Eqs. (19) and (20) (Gur and Rosen, 2009). The torque is assumed to be proportional to the difference between the electric current i and the motor no-load current i_0. The counter-electromotive force is assumed to be proportional to the rotational speed. Both equations make use of constants K_Q and K_V, which are motor properties.

$$Q_m = (i - i_0)/K_Q \tag{19}$$

$$U_m = \Omega/K_V \tag{20}$$

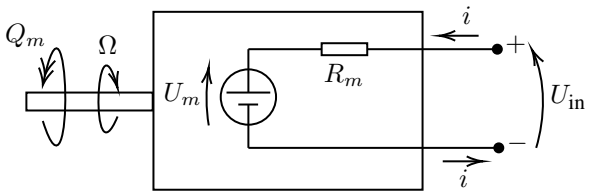

Figure 1. Electric motor circuit diagram.

3. PERFORMANCE ANALYSIS

3.1 Cruise Equilibrium and Thrust

The cruise phase takes place at a defined altitude h, with constant velocity V. In this phase, the equilibrium conditions are given by Eqs. (1) and (2). Rearranging the terms in Eq. (2) yields the expression for the the lift coefficient required to fly at h and V, as shown in Eq. (21).

$$C_L = \frac{2W}{\rho V^2 S} \tag{21}$$

Since the cruise phase is characterized by straight and level flight, the flightpath angle γ is zero, hence Eq. (1) is reduced to:

$$T = D \tag{22}$$

Equation (22) shows that in cruise flight, the required thrust is equal to the drag, which can be calculated with Eq. (4) using the lift coefficient obtained from Eq. (21). Substituting Eqs. (6) and into Eq. (22) yields:

$$\rho\, C_T \left(\frac{\Omega}{2\pi}\right)^2 d^4 = D \tag{23}$$

Substituting the result of Eq. (8) (expression for C_T) into Eq. (23) and rearranging the terms results in:

$$\left(\frac{\rho c_T d^4}{4\pi^2}\right)\Omega^2 + \left(\frac{\rho b_T d^3 V}{2\pi}\right)\Omega - \left(\rho a_T d^2 V^2 + D\right) = 0 \tag{24}$$

Equation (24) is quadratic for Ω, and has a discriminant given by:

$$\Delta_T = \frac{\rho^2 V^2 d^6 b_T^2}{4\pi^2}\left[1 + \frac{4c_T}{b_T^2}\left(a_T + \frac{D}{\rho V^2 d^2}\right)\right] \tag{25}$$

By observing the expression in Eq. (25) one can conclude that $\Delta_T \geq 0$ for any value of V, hence Eq. (24) always has two real roots. Moreover, the roots have opposite signs, since the independent term in Eq. (24) is negative and the coefficient of Ω^2 is positive. The positive root is given by the following expression:

$$\Omega = \frac{\pi V}{d\, c_T}\left[|b_T|\sqrt{1 + \frac{4c_T}{b_T^2}\left(a_T + \frac{D}{\rho V^2}\right)} - b_T\right] \tag{26}$$

Equation (26) gives the parametric expression for the rotational speed in rad$/$s required to trim the aircraft at the given values of h and V.

3.2 Fuel and Oxidizer Consumption

The rotational equilibrium is achieved when the torque load applied by propeller equals the motor torque. This condition is expressed in Eq. (27):

$$Q_m = Q_{\text{pr}} \tag{27}$$

With the Ω value obtained with the expression in Eq. (26), the propeller torque is determined with Eqs. (7) and (9). Substituting the expression in Eq. (19) and the calculated value for Q_{pr} into the rotational equilibrium condition in Eq. (27) results in a parametric expression for the electric current i, as shown in Eq. (28).

$$i = K_Q \cdot Q_{\text{pr}}(\Omega, V) + i_0 \tag{28}$$

Substituting the result of Eq. (28) into Eq. (18) yields the expression for the instantaneous fuel and oxidizer mass flow:

$$\dot{m} = \left(\frac{M_{\mathrm{H_2}}}{2F\eta_{\mathrm{ano}}} + \frac{M_{\mathrm{O_2}}}{4F\eta_{\mathrm{cat}}} \right) \left(K_Q \cdot Q_{\mathrm{pr}}(\Omega, V) + i_0 \right) \tag{29}$$

The total fuel and oxidizer mass m_f is obtained by integrating the instantaneous mass flow over time:

$$m_f = \int_{t_0}^{t_f} \dot{m}\, dt \tag{30}$$

The by-product of the chemical reactions inside the fuel cell is water, which is assumed to be kept inside the aircraft fuselage. Although eliminating water could gradually reduce weight, the escape ducts an plumbing would have to be heated in order to prevent freezing. This would require a considerable amount of electric power, which could offset the beneficial effects of water elimination. Therefore, for the sake of simplicity the aircraft weight W is kept constant. Since the aircraft is assumed to fly at constant altitude and velocity, the required power is constant and so is the electric current. Hence, the integral in Eq. (30) can be simplified:

$$m_f = \dot{m} \cdot (t_f - t_0) \tag{31}$$

For a defined range s, the time interval is such that $t_f - t_0 = s/V$, and so the expression for the total fuel and oxidizer mass becomes:

$$m_f = \frac{s}{V} \left(\frac{M_{\mathrm{H_2}}}{2F\eta_{\mathrm{ano}}} + \frac{M_{\mathrm{O_2}}}{4F\eta_{\mathrm{cat}}} \right) \left(K_Q \cdot Q_{\mathrm{pr}}(\Omega, V) + i_0 \right) \tag{32}$$

4. RESULTS AND DISCUSSION

4.1 Example Aircraft and Propulsion System

A virtual aircraft model will be used to illustrate the method explained in this article. The vehicle is a general aviation twin-seat motor glider loosely based on the Schleicher ASK-21, which presents a high aerodynamic efficiency. The relevant aircraft geometric and aerodynamic parameters are shown in Table 1. The aircraft drag polar is presented in Fig. 2.

Table 1. Example aircraft geometric and aerodynamic parameters.

Parameter	Value	Unit
Wing span (b)	17	m
Wing reference area (S)	17.95	m^2
Wing aspect ratio (A)	16.10	–
Max. take-off weight (MTOW)	600	kgf
Wing loading at MTOW	33.426	$\mathrm{kgf/m}^2$

The relevant electric motor and fuel cell data are shown in Table 2. The fuel cell cathode and anode reaction yield factors are functions of the oxidizer and fuel temperature, pressure and flow. Due to the lack of more accurate data about a particular fuel cell model, the yield factors are assumed to be constant. This however does not impact the method presented in this article.

Table 2. Relevant electric motor and fuel cell data.

Parameter	Value	Unit
Motor torque constant (K_Q)	1.333	$\mathrm{A/N \cdot m}$
Motor no-load current (i_0)	220	mA
Cathode reaction yield factor (η_{cat})	0.8	–
Anode reaction yield factor (η_{ano})	0.8	–

The aircraft is assumed to be equipped with a fixed pitch, two-blade propeller, with a diameter of 1.80 m. The dimensionless parameters that the define the propeller characteristic curves are given in Table 3.

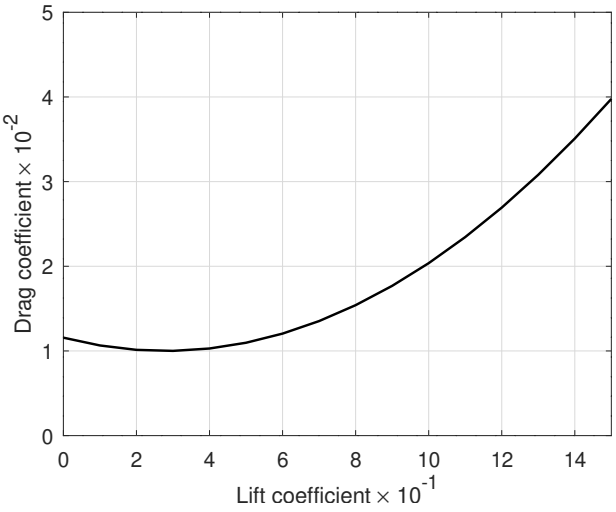

Figure 2. Example aircraft drag polar.

Table 3. Propeller dimensionless parameters.

Thrust curve parameters		Torque curve parameters	
a_T	6.29×10^{-2}	a_Q	1.45×10^{-2}
b_T	-3.37×10^{-2}	b_Q	9.96×10^{-3}
c_T	9.83×10^{-2}	c_Q	5.75×10^{-3}

4.2 Numerical Results

The parametric model presented in Sec. 4.1 is employed to provide some relevant numerical figures. The aircraft is assumed to be flying at a constant altitude of 2440 m (8000 ft) above mean sea level, which is a typical cruising altitude for general aviation airplanes. The procedures described in Sec. 3. are executed for each value of true airspeed selected from a pre-defined range. Figure 3 shows the necessary propeller rotation, in rpm, to trim the aircraft for a given velocity V, and the electric current in A consumed by the motor, also as a function of V.

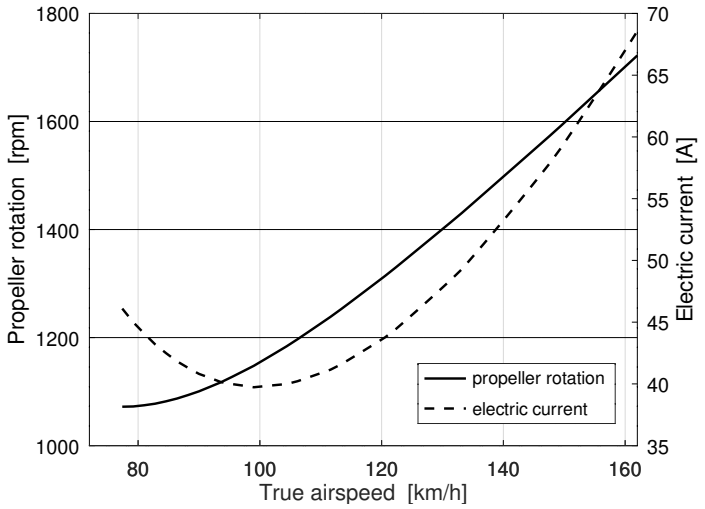

Figure 3. Propeller rotation, in rpm, and electric current consumed, in A, as functions of the true airspeed (velocity V), for cruise flight at 2440 m (8000 ft) above sea level.

The propeller rotation required increases as V increases, which is expected, since T has to increase, according to

Eqs. (22) and (4). However, the electric current does not follow the same pattern, decreasing in the beginning and then increasing again. Therefore, there is a velocity for which the electric current consumed is minimum. This results from the fact that the both the aerodynamic and propeller efficiencies have maximum values (Anderson, 1999) – in this particular case, the maximum efficiencies occur at different velocities.

At the given altitude, and for each value of V, the instantaneous consumption (mass flows) of fuel and oxidizer are calculated with Eqs. (16) and (17), respectively. Figure 4 shows the mass flows as functions of V. Since $\dot{m}_{\mathrm{H}_2}$ and $\dot{m}_{\mathrm{O}_2}$ are directly proportional to the electric current, they too present minimum values.

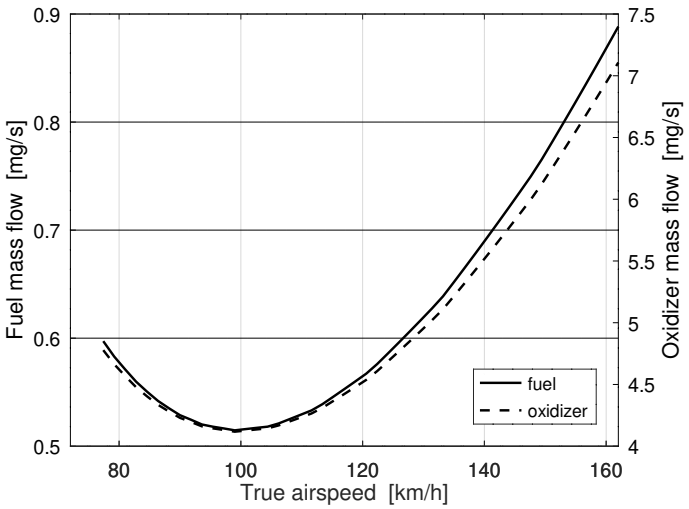

Figure 4. Mass flows (instantaneous consumption) of fuel and oxidizer, as functions the true airspeed (velocity V), for the reference altitude.

In order to analyze the total fuel and oxidizer consumption, a short-range flight is defined, with a 250 km straight path. The total consumption m_f is calculated according to Eq. (32), for each value of V. Figure 5 shows the total fuel and oxidizer consumption as a function of the airspeed.

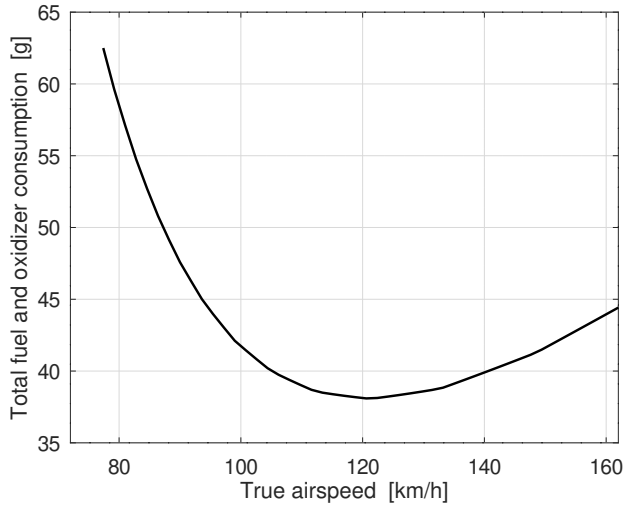

Figure 5. Total fuel and oxidizer consumption, in grams, as a function the true airspeed (velocity V), for a cruise flight of 250 km at the reference altitude.

Figure 5 shows that the total consumption curve also has a minimum. However, this point occurs at a higher velocity. Although the instantaneous consumption reaches the minimum value at a lower velocity, the total travel time decreases as the velocity increases. Since m_f is the product between the total time and the total instantaneous consumption, the minimum is moved to a higher velocity.

It is worth mentioning that the total consumption for the flight is very low in terms of mass. This is due to a high aerodynamic efficiency, and also to the fact that the fuel and oxidizer present high energy density. However, both sub-

stances have low densities and, depending on the temperature, the volumes may be significant. Moreover, the storage of H_2 and O_2, whether in liquid or gaseous form, requires a considerable amount of space and weight, especially if the storage system is cryogenic. Although fuel cells are more efficient than batteries regarding the fuel and oxidizer masses, the storage equipment required to keep the substances can be heavy and cumbersome, which may offset this particular advantage.

5. CONCLUSIONS

This work has presented a method based on analytical procedures for computing the fuel and oxidizer consumption during the cruise flight of all-electric aircraft powered by fuel cells. Analytical expressions for fuel consumption were derived and presented in parametric form for steady flight condition. These formulas allow quick calculations and do not require numerical solvers, which is convenient, especially during the conceptual design phase. The parametric form is also useful for studies involving different aircraft design variables. An example aircraft model was presented in parametric form, with relevant data about the propulsion system, including the propeller. To illustrate the method developed in the article, numerical results were obtained using the expressions presented. A cruising flight condition was defined, taking place at 8000 ft, with different velocity values within a predefined range. The propeller rotation values required to trim the aircraft were calculated, together with the associated electric current consumed by the motor. Then the fuel and oxidizer mass flows were obtained, and also the total mass consumed in a short-range flight of 250 km. The results showed that there is a velocity for which the electric current is minimum and, therefore, the instantaneous consumption of fuel and oxidizer is also minimum. For the short-range flight, the total consumption was found to also have a minimum point, however at a higher velocity, due to the decreasing travel time. The results for the total consumption also showed that electric aircraft powered by fuel cells can be very fuel-efficient, which is a crucial advantage in the current search for "greener" airplanes.

6. ACKNOWLEDGEMENTS

This study was financed in part by the Coordenação de Aperfeiçoamento de Pessoal de Nível Superior – Brasil (CAPES) – Finance Code 001, under the research grant number 88882.180826/2018-01.

7. REFERENCES

Anderson, J.D., 1999. *Aircraft Performance and Design*. McGraw-Hill, New York, 1st edition.

Boeing, 2015. "Here's Watts Up: We've Got the Power". The Boeing Company. URL `http://www.boeing.com/features/2015/01/corp-hybrid-01-05-15.page`. Retrieved 4 Jun. 2018.

Caldwell, A., 2020. "Why hydrogen cars will be Tesla's biggest threat". Business Insider. URL `https://www.businessinsider.com/hydrogen-fuel-cell-cars-teslas-biggest-threat-2019-12`.

DLR, 2016. "Zero-emission air transport – first flight of four-seat passenger aircraft HY4". Deutsches Zentrum für Luft- und Raumfahrt e.V. URL `https://www.dlr.de/dlr/en/desktopdefault.aspx/tabid-10081/151_read-19469/#/gallery/24480`. Retrieved 8 Jun 2018.

Gur, O. and Rosen, A., 2009. "Optimizing electric propulsion systems for unmanned aerial vehicles". *Journal of Aircraft*, Vol. 46, No. 4, pp. 1340–1353. doi:10.2514/1.41027.

Keane, A.J., Sóbester, A. and Scanlan, J.P., 2017. *Small Unmanned Fixed-wing Aircraft Design: A Practical Approach*. Wiley, Hoboken, 1st edition.

Kelly, T.J., 2001. *Moon Lander – How we developed the Apollo Lunar Module*. Smithsonian Books, Washington.

Lapeña-Rey, N., Mosquera, J., Bataller, E. and Ortí, F., 2010. "First Fuel-Cell Manned Aircraft". *Journal of Aircraft*, Vol. 47, No. 6, pp. 1825–1835. doi:10.2514/1.42234.

Mises, R.V., 1945. *Theory of Flight*. Dover Publications, New York. Pp. 285-316.

NASA/NOAA/USAF, 1976. *U.S. Standard Atmosphere, 1976*. National Aeronautics and Space Administration, National Oceanic and Atmospheric Administration, United States Air Force.

Nelson, R.C., 1998. *Flight Stability and Automatic Control*, McGraw-Hill, New York, pp. 96–161. 2nd edition.

O'Hayre, R., Cha, S.W., Colella, W. and Prinz, F.B., 2009. *Fuel Cell Fundamentals*. Wiley, Hoboken, 2nd edition.

Sachs, G., 2012. "Flight Performance Issues of Electric Aircraft". In *AIAA Atmospheric Flight Mechanics Conference*. doi:10.2514/6.2012-4727.

Schemp-Hirth, 2012. "The Arcus-E Sailplane". Schempp-Hirth Flugzeugbau GmbH. URL `https://www.schempp-hirth.com/en/sailplanes/arcus/arcus-e.html`. Retrieved 10 Nov 2019.

8. RESPONSIBILITY NOTICE

The authors are solely responsible for the printed material included in this paper.